# Secondary Coordination Effects of Adjacent Metal Center in Metal-Nitrogen-Carbon Improve Scaling Relation of Oxygen Electrocatalysis

Ke Ye[a,b†], Yulan Han[c†], Min Hu[a]*, P. Hu[c,d], Mårten S. G. Ahlquist[b]*, Guozhen Zhang[a,e]*

[a] Hefei National Research Center for Physical Sciences at the Microscale, School of Chemistry and Materials Science, University of Science and Technology of China, Hefei, Anhui 230026, China.
[b] Department of Theoretical Chemistry and Biology, KTH Royal Institute of Technology, 10691 Stockholm, Sweden
[c] School of Chemistry and Chemical Engineering, Queen's University Belfast, Belfast BT9 5AG, U.K.
[d] School of Physical Science and Technology, ShanghaiTech University, Shanghai 201210, China.
[e] School of Future Technology, University of Science and Technology of China, Hefei, Anhui 230026, China.

## Abstract

Heterogenous single-atom catalysts (SACs) are reminescent of homogenous catalysts because of similarity of structural motif of active sites, showing the potential of using the advantage of homogenous catalysts to tackle challenges in hetereogenous catalysis. In heterogeneous oxygen electrocatalysis, the homogeneity of adsorption patterns of reaction intermediates leads to scaling relationships that limit their activities. In contrast, homogeneous catalysts can circumvent such limits by selectively altering the adsorption of intermediates through secondary coordination effects (SCE). This inspired us to explored potential SCE in metal-nitrogen-carbon (M-N-C), a promising type of oxygen evolution electrocatalysts. We introduced SCE with a neighboring metal site, which can modulate the adsorption strengths of oxygen-containing intermediates. First-principles calculations show that the second site in heteronuclear duo four-nitrogen-coordinated metal-center can induce SCE that selectively stabilize the OOH intermediate, but with minor effects on the OH intermediate, and thereby, disrupt scaling relation between oxygen-species, and eventually increase the catalytic activity

in oxygen evolution reactions. Additionally, the activity of oxygen reduction reaction of selected M-N-C is also enhanced by such SCE. Our computational work underscored the critical role SCE can have in shaping activities of SACs, particularly in altering scaling relationships favorably, and demonstrated its potential of addressing catalytic challenges in heterogeneous catalysis.

The emergence of single-atom catalysis (SACs)[1] not only paves a path for creating a new type of heterogeneous catalysts that combines high activity and economic utilization of transition metal atoms, but also provides a promising architecture of catalyst that can fuse advantages of conventional heterogeneous and homogeneous catalysts[2-6]. In the past decade, with the aid of sophisticated experimental techniques and computational tools, scientists have made substantial progress in both crafting well-controlled structures and understanding the working mechanisms of SACs[7-13]. There is no doubt that the local environment around metal centers in SACs plays a crucial part in shaping their electronic structures and ensuing catalytic activity and selectivity[3, 9, 12], including the coordinating atoms of metal centers[7, 14], the multi-adsorption effects[15-17], and the strength of metal-support interaction[18]. While most of these studies have primarily focused on the first coordination layer[4, 8, 10-12, 19], much less attention has been paid to the secondary[20] and even more distant coordination shells of metal centers in SACs. Meanwhile, in enzymatic and homogeneous catalysis, the secondary coordination shell is known to play an important role in determining the performance of the catalyst of interest[21-27]. Even though SACs may share some similarity with molecular catalysts regarding to the structures of active centers, and some earlier work has shown the cooperation of two adjacent active sites[28-29] , there has been little computational investigation exclusively on the secondary coordination effects in SACs.

For heterogeneous catalysis, it is well established that scaling relationships between the adsorption energies of intermediates limit the performance of a catalysts, including nitrogen reduction reaction (NRR), $CO_2$ reduction reaction ($CO_2$RR), oxygen evolution reaction (OER), and oxygen reduction reaction (ORR)[13, 26, 29-33]. Taking

OER and ORR on transition metal surfaces as examples, the universal scaling relationship between the adsorption energies of key intermediates(*OH, *O, and *OOH), represented by $\Delta G_{*O} = 2\Delta G_{*OH}$ and $\Delta G_{*OOH} = \Delta G_{*OH} + 3.2$, set a theoretical limit of the overpotential at 370 mV for the most active metal[34]. Highly active single-sites in SACs cannot be free from these scaling relations as well[28-29, 35]. It mainly originates from the homogeneity of the adsorption of intermediates, meaning that the adsorption site and pattern of different intermediates are not changed during the reaction process[36]. Meanwhile, enzymes and molecular catalysts can break the homogeneity of adsorption and bypass the limit with the help of the secondary coordination ligands, by selectively tunning the adsorption of intermediates or even changing the mechanism from water nucleophilic attack (WNA), where water attacks a metal oxo speices, to coupling two metal-oxo entities (I2M), where two metal oxyl radicals form the O-O bond. Craig et al. found that the intramolecular H-bonding between *OOH and the coordinating ligands in Ru complexes could selectively stabilize *OOH intermediate and result to a lower value of $\Delta G_{*OOH} - \Delta G_{*OH}$, which is favorable for OER[26]. Matheu et al. showed that H-bonding between dangling carboxylate group and *OOH can boost the kinetics of the *O to *OOH step in the WNA mechanism [37]. Theoretical investigations have also predicted that the second coordination sphere could modulate the binding energy of the crucial *O intermediate[27]. More drastic effect can be found when the secondary interactions change the mechanism of OER. For example, Zhang et al. reported that the carboxylate groups in $Ru(tda)(py)_2$(tda = (2,2′:6′,2″-terpyridine)-6,6″-dicarboxylate, py = pyridine), can work as an oxide relay in catalytic water oxidation, which will replace the OOH intermediate with a per-carboxylate species[38-40]. Therefore, identifying the secondary coordination effects (SCE) in SACs by means of theoretical computation may help us sort out how to leverage it to alter scaling relations in heterogeneous catalysis towards improved activities.

To test our hypothesis about SCE in SACs, we chose OER and ORR as the reactions of interest because of their well-estabilished scaling relations and the associated difficulty of changing them. We used the metal-nitrogen-carbon (M-N-C)

materials in which $MN_4$ fragments are anchored in the plane of defected graphene as model SACs thanks to the ease of synthesis[41-42] and their potential of being cost-effective OER and ORR catalysts[43-44]. Through periodic spin-polarized density-functional theory calculations, we found that SCE can disrupt the scaling relationships of OER and ORR in two ways: (1) SCE disrupt the scaling relation between $\Delta G_{*O}$ and $\Delta G_{*OH}$ ($\Delta G_{*O} = 2\Delta G_{*OH}$ on the pure metal surface[30, 34] ); (2) SCE selectively stabilizes *OOH without strengthening the adsorption of *OH, which decreases the free energy change from *OH to *OOH ($\Delta G_{*OOH} = \Delta G_{*OH} + 3.2$ eV on the pure metal surface [30, 34], and the ideal intercept is 2.46 eV). As a result, we obtained more favorable energetics of OER and ORR, which could convert into better turnover-frequencies, as supported by a microkinetics simulation. Our study demonstrates the significance of exploring the secondary coordination effects in heterogeneous SACs and leveraging them for enhanced catalytic performances.

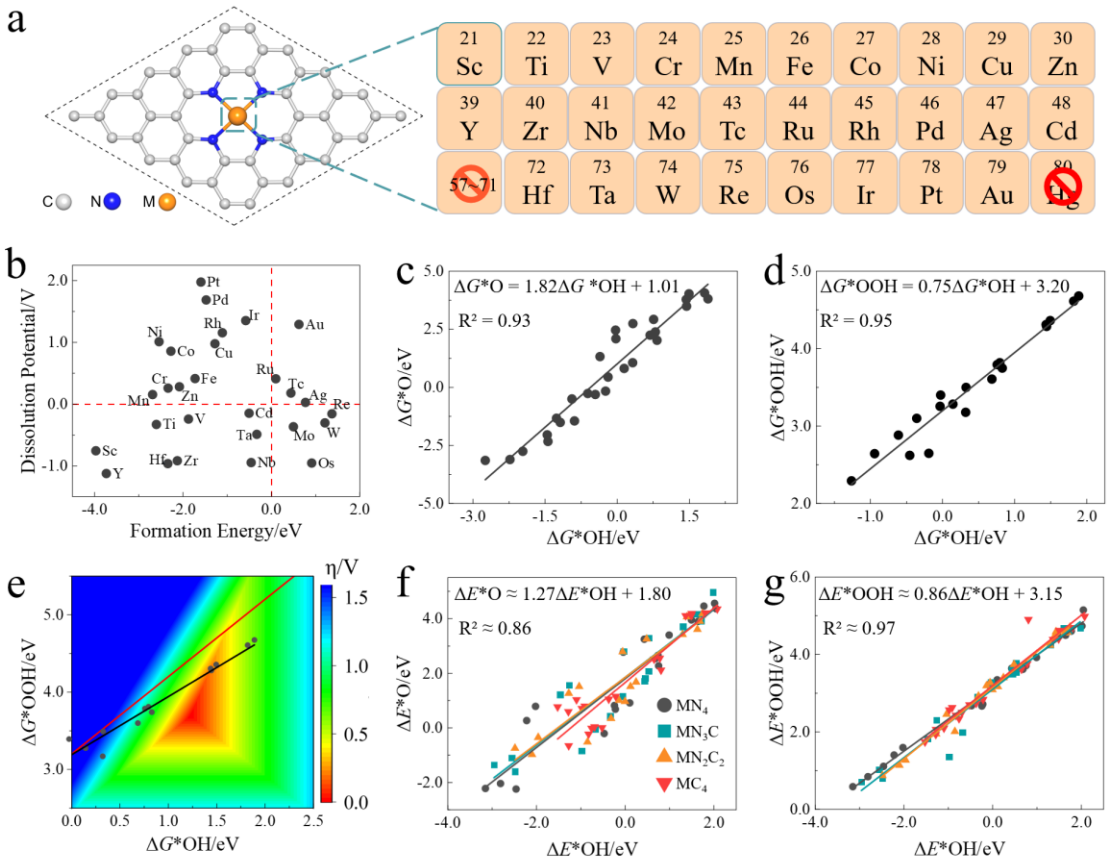


Figure 1. a) The structural prototype of $MN_4$/G. b) formation energy and dissolution potential of $MN_4$/G. c) the scaling relationships between $\Delta G_{*O}$ and $\Delta G_{*OH}$. d) the scaling relationships between $\Delta G_{*OOH}$ and $\Delta G_{*OH}$. e) 2-D volcano plot for OER, the red line represents the scaling relationship

between *OOH and *OH on metals($\Delta G_{*OOH}=\Delta G_{*OH}+3.2$), and the black line represents the scaling relationship between *OOH and *OH on $MN_4$/G. f) the scaling relationships between $\Delta E_{*O}$ and $\Delta E_{*OH}$ on $MN_xC_{4-x}$/G(x=0, 2, 3, 4). g) the scaling relationships between $\Delta E_{*OOH}$ and $\Delta E_{*OH}$ on $MN_xC_{4-x}$/G(x=0, 2, 3, 4).

We first built 28 different types of M-N-C models (denoted as $MN_4$/G) differing by the element of metal center (Figure 1a), some of which have been reported in both experimental and theoretical studies[4, 45]. Then the thermodynamic and electrochemical stabilities of these $MN_4$/G structures were assessed by formation energy and dissolution potential[28, 46]. Those in the upper left zone of Figure 1b (negative formation energy and positive dissolution potential) are energetically more favorable, covering many experimentally synthesized $MN_4$/G SACs (M=Fe, Ni, Cu, Zn, Ru, Rh, Pd, and Ir)[42]. As Figures 1c and 1d show, $MN_4$/G have only shown limited improvement in scaling relations between $\Delta G_{*OH}$ and $\Delta G_{*OOH}$ than pure metal surfaces[34]. The main reason lies in the large intercept value (3.2 eV) in the scaling equation ($\Delta G_{*OOH}=0.75\Delta G_{*OH}+3.2$) favors a weaker binding of *OOH. An incremental tuning the first coordination shell of $MN_4$ site ($MN_3C$/G, $MN_2C_2$/G, and $MC_4$/G) by replacing N atoms with C atoms does not make significant change (Figures 1f and 1g), suggesting that fine-tuning first coordination shell may be ineffective in altering scaling relations in OER. Note that we used adsorption energies instead of adsorption free energies in the test of variants of $MN_4$/G, because the difference between these two energy terms is contributed by zero-point energy and entropy item of adsorbates, which we expect are comparable before and after the adsorption and will not appreciably affect the scaling relations.

Then we expanded the scope of investigation to the seconcary coordination shell of a metal center by employing a dual active-center model (shorted as ho-2-$MN_4$/G), which have been demonstrated to disrupt linear relationships in NRR[28, 33, 47]. However, simply introducing a second adjacent metal center just did not bring SCE that can change existing scaling relationships in OER. As shown in Figure 2a, we have categoried a total of 28 kinds of ho-2-$MN_4$/G into three groups depending on how *OOH is relaxed on metal center(s): (1) indigo group (strong adsorption): *OOH directly decomposes into *O and *OH, each of them is one of two metals; (2) orange group (medium adsorption): *OOH is on one metal center and the other is idle; (3) brick

red group (weak adsorption): *OOH bridges with two metal centers. Based on adsorption energies of groups 2 and 3, little change has been found compared to the counterpart in mono $MN_4$/G (Figure 1g), indicating the ho-2-$MN_4$/G model (Figure 2b) cannot improved the scaling relations of OER as it does on NRR. The fact that the O-O bond is less strong than a N-N bond indicates that tuning the binding strength of *OOH maybe more delicate than that of *NNH. We have examined a bunch of variants of the ho-2-$MN_4$/G model, including (1) a similar M-N-C with shorter metal-metal distances (Figures 2c and S1), and (2) other duo $MN_4$/G models (Figures S2 and S3) with different two-dimensional carbon support, such as carbon nanotube with different diameters, but all failed to obtain improved scaling relationships between $\Delta E_{*OOH}$ and $\Delta E_{*OH}$. Therefore, a pair of active centers alone will not create SCE in SACs.

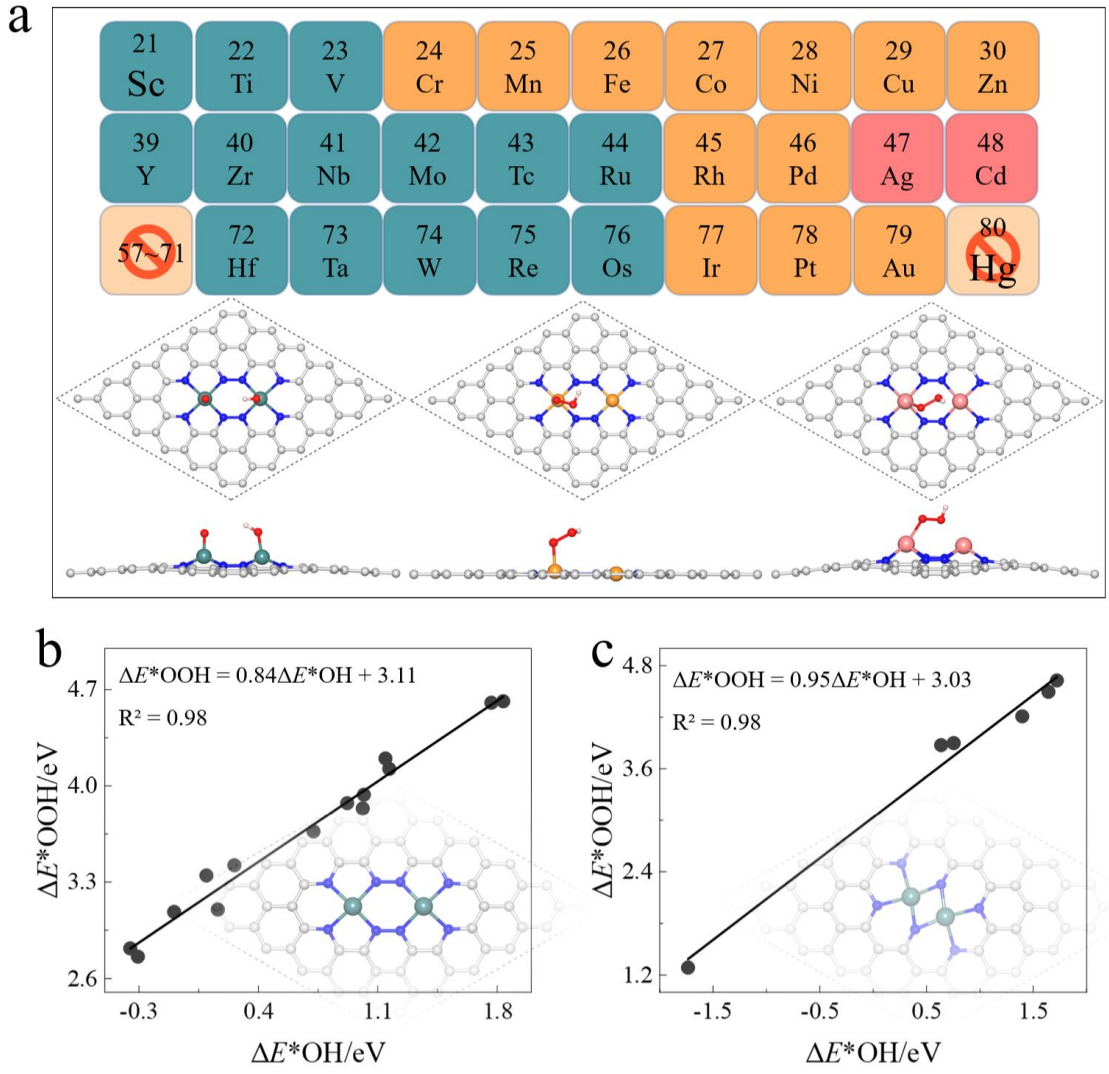


Figure 2. a) Three kinds of *OOH adsorption manners on ho-2-$MN_4$/G. b) the scaling relationships between on $\Delta E_{*OH}$ and $\Delta E_{*OOH}$ on ho-2-$MN_4$/G. c) the scaling relationships between $\Delta E_{*OH}$ and

$\Delta E_{*OOH}$ on homonuclear duo $MN_4$/G model with two $MN_4$ sites getting closer compared to ho-2-$MN_4$/G.

As shown in Figure 3a, the adsorption of OH on selected metal centers (inside indigo oval) is much stronger, which makes it thermodynamically unfavorable to be converted into *O of OER because of large ordinate value ($\Delta E_{*O}$-$\Delta E_{*OH}$). Consequently, OH may stay on these oxygen-philic metal centers, making them potential secondary coordination ligands for the adjacent metal center, similar to the secondary coordination ligands in homogeneous catalysis[26]. Then we selected 4 types of $M1N_4$ (M1= Cd, Sc, Y, and Zn) to host OH based on the relative strength of OH adsorption on each $M1N_4$, and 6 types of $M2N_4$ (M2=Ag, Co, Cu, Ir, Ni, and Rh) as potential active centers for OER. A total of 24 combinations of $M1N_4$-$M2N_4$/G, of which the thermo stability has been verified by a 20-ps ab initio molecular dynamics simulation, were generated and the corresponding adsorption energies of *OH, *O, and *OOH were calculated using the same procedure. In the presence of *OH on M1 sites (denoted as *OH(M1)), the linear scaling of adsorption free energies between *O and *OH (Figure 3b) on M2 sites is substantially weakened ($R^2$ decreased from 0.93 in $MN_4$/G to 0.54 in $M1N_4$-$M2N_4$/G). Moreover, the scaling line between *OH and *OOH (Figure 3c) shifts down, making the intercept closer to the ideal value of 2.46. Thus, the new scaling is closer to the theoretical peak in the contour map (Figure 3d), suggesting a chance of finding a more active OER catalyst in $M1N_4$-$M2N_4$/G than $MN_4$/G.

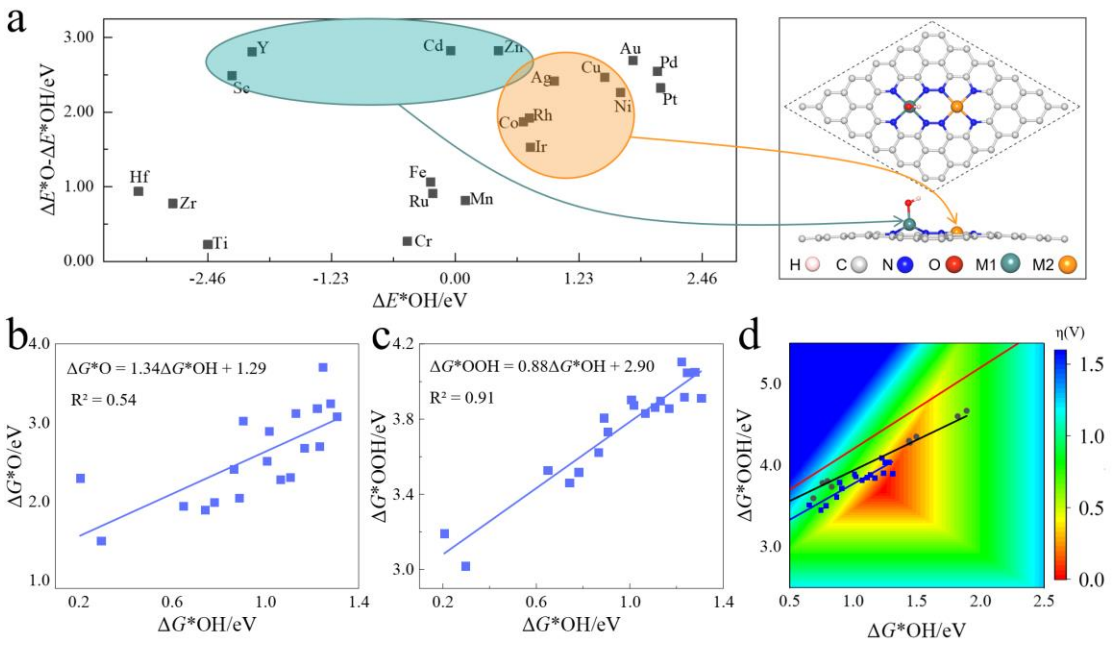


Figure 3. a) The distribution of $MN_4$/G along the $\Delta E_{*OH}$ and $\Delta E_{*O}$ - $\Delta E_{*OH}$. And the structural prototype of $M1N_4$-$M2N_4$/G at the right side. b) the scaling relationship between $\Delta G_{*OH}$ and $\Delta G_{*O}$ on $M1N_4$-$M2N_4$/G. c) the scaling relationship between $\Delta G_{*OH}$ and $\Delta G_{*OOH}$ on $M1N_4$-$M2N_4$/G. d) 2-D volcano plot for OER, the red line represents the scaling relationship for $\Delta G_{*OOH}$ and $\Delta G_{*OH}$ on metals, the black line represents the scaling relationship for $\Delta G_{*OOH}$ and $\Delta G_{*OH}$ on $MN_4$/G, and the blue line represents the scaling relationship for $\Delta G_{*OOH}$ and $\Delta G_{*OH}$ on $M1N_4$-$M2N_4$/G.

Following the improvement of the scaling relationship between *OH and *OOH from $MN_4$/G to $M1N_4$-$M2N_4$/G, we conducted a more comprehensive kinetics analysis based on energetic data of every step in OER process, to examine that if SCE enhanced $M1N_4$-$M2N_4$/G by *OH(M1) is potentially a better OER catalyst than $MN_4$/G. The details of microkinetics calculations using the CatMAP software package[48] have been provided in the supporting information. Since the contour map of $M1N_4$-$M2N_4$/G (Figure 4b) not only has more data points closer to the peak than $MN_4$/G (Figure 4a) but also possesses a substantially larger area with noticeable OER activity, it is more likely to locate an efficient OER catalyst within $M1N_4$-$M2N_4$/G than $MN_4$/G, thus supporting our hypothesis about the promotive SCE role of *OH(M1) on OER.

To further validate whether SCE can effectively enhance OER catalytic performance occurring on $M1N_4$-$M2N_4$/G, we calculated the free energy diagrams covering the full set of elementary steps on six of the selected model systems (Figure

4c). Compared each $MN_4$/G, the counterpart $M1N_4$-$M2N_4$/G enjoys varying degrees of decrease of overpotential with the aid of *OH(M1). Among these $M1N_4$-$M2N_4$/G systems, *OH(Sc) gives $NiN_4$/G the largest improvement (a decrease by 0.57 V) in overpotential, and *OH(Zn) gives $IrN_4$/G the lowest overpotential of 0.24 V. For the reverse reaction of OER, i.e. ORR, the SCE of *OH(M1) will also enhance the ORR activity, as illustrated in Figure S4. The best combination is $ScN_4$-$RhN_4$/G with an overpotential of 0.22 V in ORR, in which the secondary ligand OH binds to Sc.

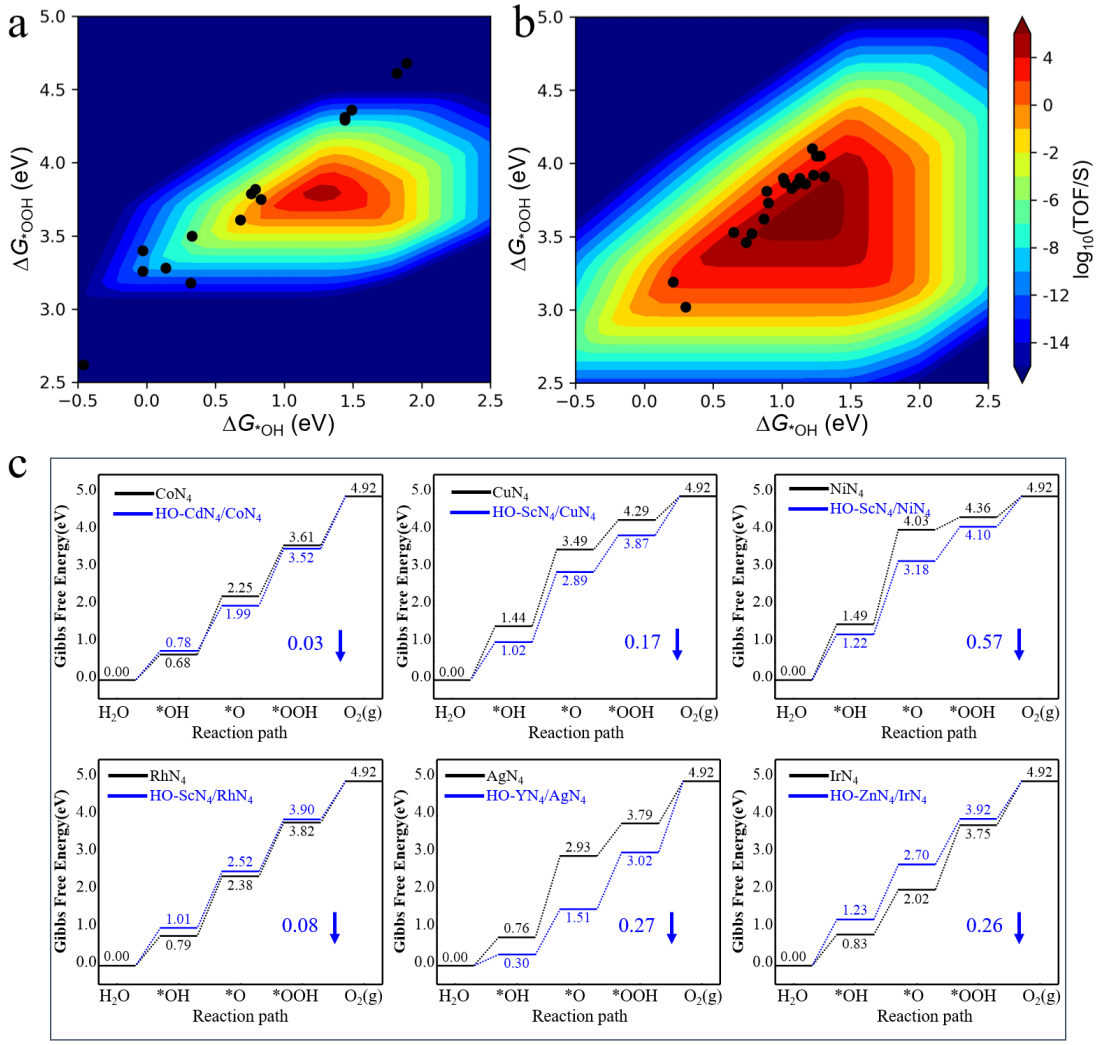


Figure 4. Oxygen evolution catalytic activity volcano maps on different active sites. Calculated OER rates as a function of the *OH adsorption energy and *OOH energy on (a) $MN_4$/G sites; b) $M1N_4$-$M2N_4$/G sites; c) Gibbs free energy diagrams of $CoN_4$/G, $CuN_4$/G, $NiN_4$/G, $RhN_4$/G, $AgN_4$/G and $IrN_4$/G and the respective corresponding $M1N_4$-$M2N_4$/G for OER. The blue downward arrows and adjacent numbers indicate the reduction in the OER overpotential on $M1N_4$-$M2N_4$/G sites (blue line) compared with the $MN_4$/G sites (black line).

Finally, we investigated how SCE of *OH(M1) alters the free energy diagram of OER on $M2N_4$. Overall, the presence of *OH(M1) next to M2 tends to equalize the free energy change of consecutive elementary steps (Figure 4c). For the step of *O formation, the much weaker scaling relationship between *OH and *O (Figure 3b) in the presence of *OH(M1) makes the corresponding free energy changes generally more favorable for smaller overpotentials. To understand the change, we calculated the integrated crystal orbital Hamilton population (ICOHP) between M2 and O of *OH with and without adjacent *OH-M1, for which more negative value indicates stronger bonding. As Figure 5a shows, for $CuN_4$, $IrN_4$, and $NiN_4$, the presence of *OH(M1) appreciably affects the bonding strength between M2 and O of *OH. Taking $CuN_4$ as an example, the ICOHP between O and Cu atom is -1.17 for *OH on single $CuN_4$, and increased to -1.78 in the presence of another *OH on the adjacent $ScN_4$ site. For the step of *OOH formation, *OH(M1) can selectively stabilize *OOH(M2) by forming either bridge-on adsorption of OOH with both M1 and M2 or hydrogen bonds between *OH(M1) and *OOH(M2) (Figure 5b). Either way, *OH(M1) helps alter the scaling relation between *OH and *OOH by lowering the intercept, which favors the thermodynamics of OER. Similar ICOHP analysis has been done on $CoN_4$ and $RhN_4$ (Figure S5), in which *OH(M1) also sways the energetics of *OH in a favorable way. This geometry-based SCE for *OH(M1) is reminiscent of the promotion role of secondary ligands in enzymatic and homogeneous catalysts. Therefore, by carefully considering the local environment around active centers in high-density SACs, we can leverage the SCE to modulate their catalytic activities.

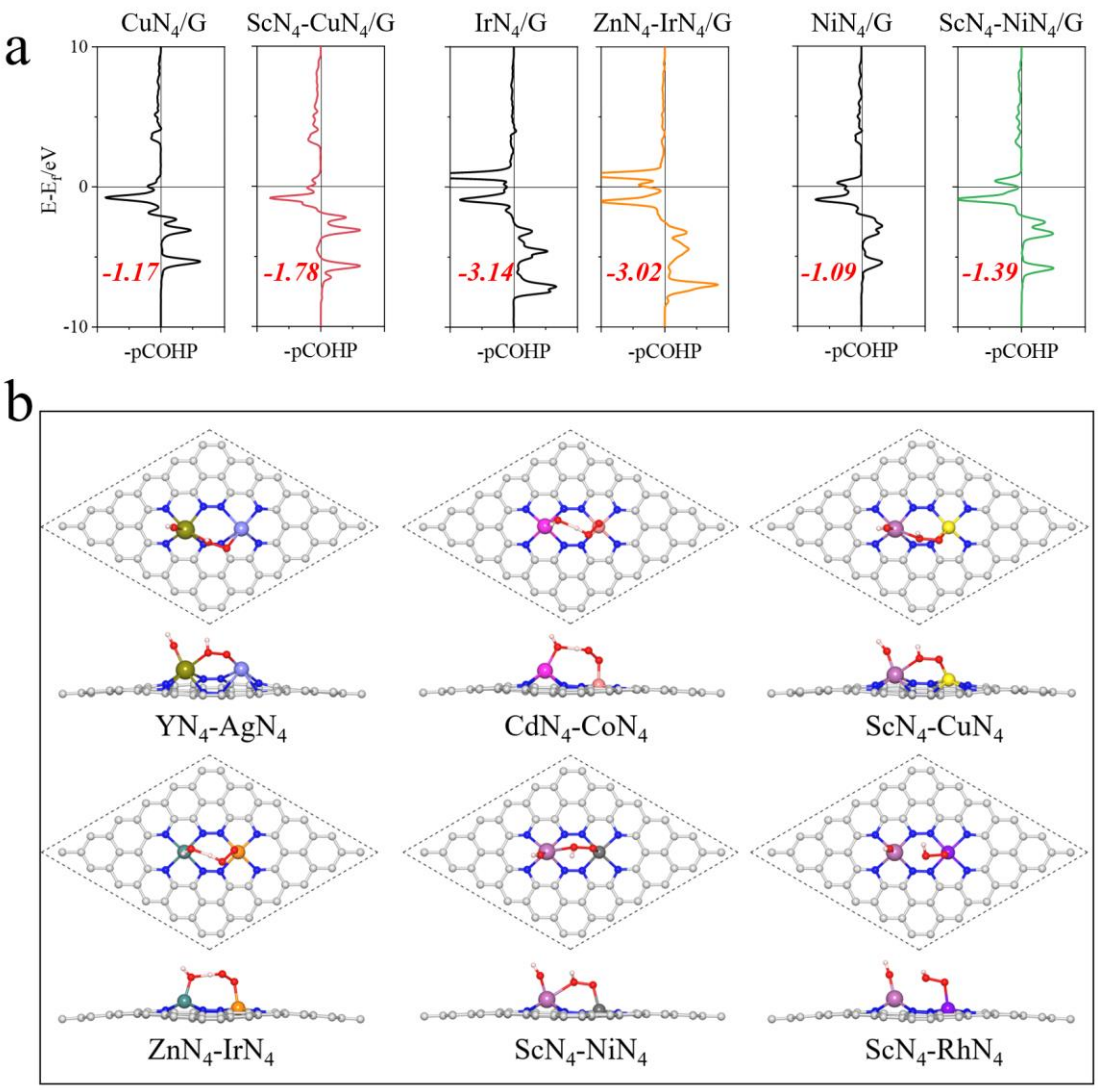


Figure 5. a) Projected crystal orbital Hamilton population (pCOHP) between the metal centers and the oxygen atom in *OH intermediate. The values of integrated COHP (ICOHP) are shown in red bold italics; b) Adsorption configurations of *OOH on M2 in $M1N_4$-$M2N_4$/G models.

In summary, our work introduced the concept of secondary coordination environments prevailing in molecular catalysts into heterogeneous SACs and showed the impact of secondary coordination effects on the scaling relationships between intermediates (*OH, *O and *OOH) of OER and ORR. The axial OH bound to the oxygen-philic metal of heteronuclear duo $MN_4$/G catalysts acts as a secondary ligand of active center, alters the scaling relations that shape the theoretical limit of OER and ORR activities on these model systems, and finally leads to improved activities for both OER and ORR. The kinetic simulation results supported the effectiveness of this strategy. Furthermore, the reduction of overpotentials of OER and ORR shown by free

energy diagrams is ascribed to the effect of this adjacent axial OH ligand. The computational results disclosing the role of SCE in model SACs offer new insight into the modulation of M-N-C type OER and ORR catalysts, which will provide sparks of the rational design of SACs with enhanced activities in oxygen electrocatalysis[49] for sustainable energy development. In addition, both previous[28-29] and current work suggest that proper engineering of the secondary coordination sites allows the heterogeneity of binding modes for different intermediates, which is critical for modifying the linear scaling relationship of their adsorption strengths. Therefore, we expect that the modulation of secondary coordination sites may provide an alternative strategy to overcome the hurdle of scaling relationships in heterogeneous catalysis.

## Associated content

**Supporting Information** The Supporting Information is available free of charge and contains computational details, geometrical structures, and stability validation of $MN_4$, the adsorption energies of *OH, *O, and *OOH, various scaling relationships, and Gibbs free energy diagrams for the ORR occurring on selected $M1N_4$-$M2N_4$/G models.

## Author information

Corresponding Authors

**Guozhen Zhang**-Hefei National Research Center for Physical Sciences at the Microscale, School of Chemistry and Materials Science, University of Science and Technology of China, Hefei, Anhui 230026, China. Email: guozhen@ustc.edu.cn

**Mårten S. G. Ahlquist**-Department of Theoretical Chemistry and Biology, KTH Royal Institute of Technology, 10691Stockholm, Sweden; Email: ahlqui@kth.se

**Min Hu**- Hefei National Research Center for Physical Sciences at the Microscale, School of Chemistry and Materials Science, University of Science and Technology of China, Hefei 230026, China. Present address: Department of Chemical and Biological Engineering, Hong Kong University of Science and Technology of China, Hong Kong. Email: humin@mail.ustc.edu.cn

## Author Contributions

Ke Ye and Yulan Han contributed equally to this work.

## Acknowledgments

This work is supported by the NSFC (22273093, 92045303 and 22103018) and NKRDPC (2021YFA1500700). K.Y. and M.H. are grateful to the support from Prof. Jun Jiang. Y.H. acknowledges the financial support from the Queen's University Belfast, the China Scholarship Council and the European Union's Horizon 2020 research and innovation program under the Marie Skłodowska-Curie Grant (agreement no. 823745). The authors are grateful for computational resources from both China and UK, including Supercomputing Center of University of Science and Technology of China, the UK national high-performance computing service, ARCHER, for which access was obtained via the UKCP consortium and funded by EPSRC grant ref EP/P022561/1, the UK Materials and Molecular Modelling Hub for computational resources, which is partially funded by EPSRC (EP/P020194/1), and the Queen's University Belfast Kelvin HPC service, which is partially funded by ESPRC (EP/T022175/1).

## References

[1] Qiao, B.; Wang, A.; Yang, X.; Allard, L. F.; Jiang, Z.; Cui, Y.; Liu, J.; Li, J.; Zhang, T. Single-Atom Catalysis of CO Oxidation Using Pt1/FeOx. *Nat. Chem.* **2011**, *3*, 634-641.

[2] Li, Z.; Li, B.; Yu, C. Atomic Aerogel Materials (or Single-Atom Aerogels): An Interesting New Paradigm in Materials Science and Catalysis Science. *Adv. Mater.* **2023**, *35*, e2211221.

[3] Zhang, W.; Fu, Q.; Luo, Q.; Sheng, L.; Yang, J. Understanding Single-Atom Catalysis in View of Theory. *JACS Au* **2021**, *1*, 2130-2145.

[4] Li, J.; Stephanopoulos, M. F.; Xia, Y. Introduction: Heterogeneous Single-Atom Catalysis. *Chem. Rev.* **2020**, *120*, 11699-11702.

[5] Chen, F.; Jiang, X.; Zhang, L.; Lang, R.; Qiao, B. Single-Atom Catalysis: Bridging the Homo- and Heterogeneous Catalysis. *Chinese J.Catal.* **2018**, *39*, 893-898.

[6] Wang, A.; Li, J.; Zhang, T. Heterogeneous Single-Atom Catalysis. *Nat. Rev. Chem.* **2018**, *2*, 65-81.

[7] Li, L.; Chang, X.; Lin, X.; Zhao, Z.-J.; Gong, J. Theoretical Insights into Single-Atom Catalysts. *Chem. Soc. Rev.* **2020**, *49*, 8156-8178.

[8] Wang, Y.; Su, H.; He, Y.; Li, L.; Zhu, S.; Shen, H.; Xie, P.; Fu, X.; Zhou, G.; Feng, C.; Zhao, D.; Xiao, F.; Zhu, X.; Zeng, Y.; Shao, M.; Chen, S.; Wu, G.; Zeng, J.; Wang, C. Advanced Electrocatalysts with Single-Metal-Atom Active Sites. *Chem. Rev.* **2020**, *120*, 12217-12314.

[9] Zhuo, H.-Y.; Zhang, X.; Liang, J.-X.; Yu, Q.; Xiao, H.; Li, J. Theoretical Understandings of

Graphene-Based Metal Single-Atom Catalysts: Stability and Catalytic Performance. *Chem. Rev.* **2020**, *120*, 12315-12341.

[10] Hannagan, R. T.; Giannakakis, G.; Flytzani-Stephanopoulos, M.; Sykes, E. C. H. Single-Atom Alloy Catalysis. *Chem. Rev.* **2020**, *120*, 12044-12088.

[11] Singh, B.; Gawande, M. B.; Kute, A. D.; Varma, R. S.; Fornasiero, P.; McNeice, P.; Jagadeesh, R. V.; Beller, M.; Zbořil, R. Single-Atom (Iron-Based) Catalysts: Synthesis and Applications. *Chem. Rev.* **2021**, *121*, 13620-13697.

[12] Kraushofer, F.; Parkinson, G. S. Single-Atom Catalysis: Insights from Model Systems. *Chem. Rev.* **2022**, *122*, 14911-14939.

[13] Xu, H.; Cheng, D.; Cao, D.; Zeng, X. C. A Universal Principle for a Rational Design of Single-Atom Electrocatalysts. *Nat. Catal.* **2018**, *1*, 339-348.

[14] Ju, W.; Bagger, A.; Hao, G. P.; Varela, A. S.; Sinev, I.; Bon, V.; Roldan Cuenya, B.; Kaskel, S.; Rossmeisl, J.; Strasser, P. Understanding Activity and Selectivity of Metal-Nitrogen-Doped Carbon Catalysts for Electrochemical Reduction of CO(2). *Nat. Commun.* **2017**, *8*, 944.

[15] Cao, L.; Liu, W.; Luo, Q.; Yin, R.; Wang, B.; Weissenrieder, J.; Soldemo, M.; Yan, H.; Lin, Y.; Sun, Z.; Ma, C.; Zhang, W.; Chen, S.; Wang, H.; Guan, Q.; Yao, T.; Wei, S.; Yang, J.; Lu, J. Atomically Dispersed Iron Hydroxide Anchored on Pt for Preferential Oxidation of CO in H2. *Nature* **2019**, *565*, 631-635.

[16] Chen, Y.; Li, H.; Zhao, W.; Zhang, W.; Li, J.; Li, W.; Zheng, X.; Yan, W.; Zhang, W.; Zhu, J.; Si, R.; Zeng, J. Optimizing Reaction Paths for Methanol Synthesis from CO2 Hydrogenation Via Metal-Ligand Cooperativity. *Nat. Commun.* **2019**, *10*, 1885.

[17] Zhao, W.; Zhang, L.; Luo, Q.; Hu, Z.; Zhang, W.; Smith, S.; Yang, J. Single $Mo_1(Cr_1)$ Atom on Nitrogen-Doped Graphene Enables Highly Selective Electroreduction of Nitrogen into Ammonia. *ACS Catal.* **2019**, *9*, 3419-3425.

[18] Liu, K.; Zhao, X.; Ren, G.; Yang, T.; Ren, Y.; Lee, A. F.; Su, Y.; Pan, X.; Zhang, J.; Chen, Z.; Yang, J.; Liu, X.; Zhou, T.; Xi, W.; Luo, J.; Zeng, C.; Matsumoto, H.; Liu, W.; Jiang, Q.; Wilson, K.; Wang, A.; Qiao, B.; Li, W.; Zhang, T. Strong Metal-Support Interaction Promoted Scalable Production of Thermally Stable Single-Atom Catalysts. *Nat. Commun.* **2020**, *11*, 1263.

[19] Kaiser, S. K.; Chen, Z.; Faust Akl, D.; Mitchell, S.; Pérez-Ramírez, J. Single-Atom Catalysts across the Periodic Table. *Chem. Rev.* **2020**, *120*, 11703-11809.

[20] Liu, H.; Zou, H.; Wang, D.; Wang, C.; Li, F.; Dai, H.; Song, T.; Wang, M.; Ji, Y.; Duan, L. Second Sphere Effects Promote Formic Acid Dehydrogenation by a Single-Atom Gold Catalyst Supported on Amino-Substituted Graphdiyne. *Angew. Chem. Int. Ed.* **2023**, *62*, e202216739.

[21] Stripp, S. T.; Duffus, B. R.; Fourmond, V.; Léger, C.; Leimkühler, S.; Hirota, S.; Hu, Y.; Jasniewski, A.; Ogata, H.; Ribbe, M. W. Second and Outer Coordination Sphere Effects in Nitrogenase, Hydrogenase, Formate Dehydrogenase, and CO Dehydrogenase. *Chem. Rev.* **2022**, *122*, 11900-11973.

[22] Van Stappen, C.; Dai, H.; Jose, A.; Tian, S.; Solomon, E. I.; Lu, Y. Primary and Secondary Coordination Sphere Effects on the Structure and Function of S-Nitrosylating Azurin. *J. Am. Chem. Soc.* **2023**, *145*, 20610-20623.

[23] Trouvé, J.; Gramage-Doria, R. Beyond Hydrogen Bonding: Recent Trends of Outer Sphere Interactions in Transition Metal Catalysis. *Chem. Soc. Rev.* **2021**, *50*, 3565-3584.

[24] Wagner, A.; Sahm, C. D.; Reisner, E. Towards Molecular Understanding of Local Chemical Environment Effects in Electro- and Photocatalytic CO2 Reduction. *Nat. Catal.* **2020**, *3*, 775-

786.

[25] Berggren, G.; Adamska, A.; Lambertz, C.; Simmons, T. R.; Esselborn, J.; Atta, M.; Gambarelli, S.; Mouesca, J. M.; Reijerse, E.; Lubitz, W.; Happe, T.; Artero, V.; Fontecave, M. Biomimetic Assembly and Activation of [Fefe]-Hydrogenases. *Nature* **2013**, *499*, 66-69.

[26] Craig, M. J.; Coulter, G.; Dolan, E.; Soriano-Lopez, J.; Mates-Torres, E.; Schmitt, W.; Garcia-Melchor, M. Universal Scaling Relations for the Rational Design of Molecular Water Oxidation Catalysts with near-Zero Overpotential. *Nat. Commun.* **2019**, *10*, 4993.

[27] Baran, J. D.; Grönbeck, H.; Hellman, A. Analysis of Porphyrines as Catalysts for Electrochemical Reduction of O2 and Oxidation of H2o. *J. Am. Chem. Soc.* **2014**, *136*, 1320-1326.

[28] Ye, K.; Hu, M.; Li, Q.-K.; Luo, Y.; Jiang, J.; Zhang, G. Cooperative Single-Atom Active Centers for Attenuating the Linear Scaling Effect in the Nitrogen Reduction Reaction. *J. Phys. Chem. Lett.* **2021**, *12*, 5233-5240.

[29] Ouyang, Y.; Shi, L.; Bai, X.; Li, Q.; Wang, J. Breaking Scaling Relations for Efficient $CO_2$ Electrochemical Reduction through Dual-Atom Catalysts. *Chem. Sci.* **2020**, *11*, 1807-1813.

[30] Busch, M.; Halck, N. B.; Kramm, U. I.; Siahrostami, S.; Krtil, P.; Rossmeisl, J. Beyond the Top of the Volcano? – a Unified Approach to Electrocatalytic Oxygen Reduction and Oxygen Evolution. *Nano Energy* **2016**, *29*, 126-135.

[31] Wang, P.; Chang, F.; Gao, W.; Guo, J.; Wu, G.; He, T.; Chen, P. Breaking Scaling Relations to Achieve Low-Temperature Ammonia Synthesis through Lih-Mediated Nitrogen Transfer and Hydrogenation. *Nat. Chem.* **2017**, *9*, 64-70.

[32] Zhao, Z.-J.; Liu, S.; Zha, S.; Cheng, D.; Studt, F.; Henkelman, G.; Gong, J. Theory-Guided Design of Catalytic Materials Using Scaling Relationships and Reactivity Descriptors. *Nat. Rev. Mater.* **2019**, *4*, 792-804.

[33] Li, X.; Duan, S.; Sharman, E.; Zhao, Y.; Yang, L.; Zhuo, Z.; Cui, P.; Jiang, J.; Luo, Y. Exceeding the Volcano Relationship in Oxygen Reduction/Evolution Reactions Using Single-Atom-Based Catalysts with Dual-Active-Sites. *J. Mater. Chem. A* **2020**, *8*, 10193-10198.

[34] Kulkarni, A.; Siahrostami, S.; Patel, A.; Norskov, J. K. Understanding Catalytic Activity Trends in the Oxygen Reduction Reaction. *Chem. Rev.* **2018**, *118*, 2302-2312.

[35] Ye, K.; Hu, M.; Li, Q. K.; Han, Y.; Luo, Y.; Jiang, J.; Zhang, G. Cooperative Nitrogen Activation and Ammonia Synthesis on Densely Monodispersed Mo-N-C Sites. *J. Phys. Chem. Lett.* **2020**, *11*, 3962-3968.

[36] Fundamental Concepts in Heterogeneous Catalysis-Wiley (2014)

[37] Matheu, R.; Ertem, M. Z.; Benet-Buchholz, J.; Coronado, E.; Batista, V. S.; Sala, X.; Llobet, A. Intramolecular Proton Transfer Boosts Water Oxidation Catalyzed by a Ru Complex. *J. Am. Chem. Soc.* **2015**, *137*, 10786-95.

[38] Zhan, S.; Ahlquist, M. S. G. Dynamics and Reactions of Molecular Ru Catalysts at Carbon Nanotube–Water Interfaces. *J. Am. Chem. Soc.* **2018**, *140*, 7498-7503.

[39] Zhan, S.; Zou, R.; Ahlquist, M. S. G. Dynamics with Explicit Solvation Reveals Formation of the Prereactive Dimer as Sole Determining Factor for the Efficiency of Ru(Bda)L2 Catalysts. *ACS Catal.* **2018**, *8*, 8642-8648.

[40] Zhan, S.; De Gracia Triviño, J. A.; Ahlquist, M. S. G. The Carboxylate Ligand as an Oxide Relay in Catalytic Water Oxidation. *J. Am. Chem. Soc.* **2019**, *141*, 10247-10252.

[41] Liu, S.; Li, Z.; Wang, C.; Tao, W.; Huang, M.; Zuo, M.; Yang, Y.; Yang, K.; Zhang, L.; Chen, S.;

Xu, P.; Chen, Q. Turning Main-Group Element Magnesium into a Highly Active Electrocatalyst for Oxygen Reduction Reaction. *Nat. Commun.* **2020**, *11*, 938.

[42] Xiong, Y.; Sun, W.; Xin, P.; Chen, W.; Zheng, X.; Yan, W.; Zheng, L.; Dong, J.; Zhang, J.; Wang, D.; Li, Y. Gram-Scale Synthesis of High-Loading Single-Atomic-Site Fe Catalysts for Effective Epoxidation of Styrene. *Adv. Mater.* **2020**, *32*, e2000896.

[43] Shi, Q.; Zhu, C.; Du, D.; Lin, Y. Robust Noble Metal-Based Electrocatalysts for Oxygen Evolution Reaction. *Chem. Soc. Rev.* **2019**, *48*, 3181-3192.

[44] Ha, M.; Kim, D. Y.; Umer, M.; Gladkikh, V.; Myung, C. W.; Kim, K. S. Tuning Metal Single Atoms Embedded in Nxcy Moieties toward High-Performance Electrocatalysis. *Energy Environ. Sci.* **2021**, *14*, 3455-3468.

[45] Xu, H.; Cheng, D.; Cao, D.; Zeng, X. C. A Universal Principle for a Rational Design of Single-Atom Electrocatalysts. *Nat. Catal.* **2018**, *1*, 339-348.

[46] Guo, X.; Gu, J.; Lin, S.; Zhang, S.; Chen, Z.; Huang, S. Tackling the Activity and Selectivity Challenges of Electrocatalysts toward the Nitrogen Reduction Reaction Via Atomically Dispersed Biatom Catalysts. *J. Am. Chem. Soc.* **2020**, *142*, 5709-5721.

[47] Wang, P.; Chang, F.; Gao, W.; Guo, J.; Wu, G.; He, T.; Chen, P. Breaking Scaling Relations to Achieve Low-Temperature Ammonia Synthesis through Lih-Mediated Nitrogen Transfer and Hydrogenation. *Nat. Chem.* **2017**, *9*, 64-70.

[48] Medford, A. J.; Shi, C.; Hoffmann, M. J.; Lausche, A. C.; Fitzgibbon, S. R.; Bligaard, T.; Nørskov, J. K. Catmap: A Software Package for Descriptor-Based Microkinetic Mapping of Catalytic Trends. *Catal. Lett.* **2015**, *145*, 794-807.

[49] Huang, Z.-F.; Song, J.; Dou, S.; Li, X.; Wang, J.; Wang, X. Strategies to Break the Scaling Relation toward Enhanced Oxygen Electrocatalysis. *Matter* **2019**, *1*, 1494-1518.

TOC